Evaluating the Properties of Dissimilar Metal Welding Between Inconel 625 and 316L Stainless Steel by Applying Different Welding Methods and Consumables

AHMAD KOURDANI and REZA DERAKHSHANDEH-HAGHIGHI

The current work was carried out to characterize welding of Inconel 625 superalloy and 316L stainless steel. In the present study, shielded metal arc welding (SMAW) and gas tungsten arc welding (GTAW) with two types of filler metals (ERNiCrMo-3 and ERSS316L) and an electrode (ENiCrMo-3) were utilized. This paper describes the selection of the proper welding method and welding consumables in dissimilar metal joining. During solidification of ERNiCrMo-3 filler metal, Nb and Mo leave dendritic cores and are rejected to inter-dendritic regions. However, ERSS316L filler metal has small amounts of elements with a high tendency for segregation. So, occurrence of constitutional super-cooling for changing the solidification mode from cellular to dendritic or equiaxed is less probable. Using GTAW with lower heat input results in higher cooling rate and finer microstructure and less Nb segregation. The interface between weld metal and base metal and also unmixed zones was evaluated by scanning electron microscopy and energy dispersive X-ray (EDX) analysis. Microhardness measurements, tensile test, and Charpy impact test were performed to see the effect of these parameters on mechanical properties of the joints.

https://doi.org/10.1007/s11661-018-4469-7
© The Minerals, Metals & Materials Society and ASM International 2018

I. INTRODUCTION

DISSIMILAR metal welding (DMW) has been the subject of interest for many researchers and is widely used to join two different alloys together in various industrial applications. DMW is utilized to improve flexibility in design and application and also reduction of material costs. However, the welding of two dissimilar alloys with different thermal expansion coefficients and melting temperature is very difficult.[1,2] Previous studies show that DMW results in a complicated microstructure that can reduce a component's resistance to material degradation.[3–5]

Inconel 625 is a nickel-based solid solution superalloy with a nickel-chromium matrix. It is widely used in aerospace, marine, chemical, petrochemical industries due to its superior physical and chemical properties, *i.e.*, high strength, corrosion, and creep resistance at elevated temperatures. It is also utilized as a heat exchanger tube in ammonia cracker plants of heavy water production.[6,7] Using less expensive materials brings down the cost without compromising the efficiency. Stainless steel 316L is a less expensive structural material. It is extensively used in the oil and gas and chemical industries for its cost effective corrosion resistance and ease of fabrication. The critical issue in the joining of Ni-based superalloy and austenitic stainless steel is the selection of proper filler wire.[8]

Shah Hosseini *et al.*[9] used gas tungsten arc (GTA) welding for joining Inconel 617 and AISI 310 using nickel-based Inconel 82, Inconel 617, and 310 austenitic stainless steel. They reported the hot cracking in the HAZ of joints produced using Inconel 82 and 310 stainless steel filler metals. In another research,[10] Inconel 617 and AISI 310 alloy were joined by three different filler metals. It was found that Inconel 617 filler metal shows superior ultimate tensile strength (UTS) and elongation. Microstructural and mechanical properties of Inconel 718 and 310s austenitic stainless steel were assessed by Mortezaie *et al.*[11] They showed that Inconel 82 and 310 SS filler metals display the highest and the lowest toughness values, respectively. Gas tungsten arc welding (GTAW) of Inconel 617 and 304H stainless steel was attempted by Reference 12 using Inconel 617 as filler metal. They showed that

AHMAD KOURDANI is with the Department of Materials Science and Engineering, Bandar Abbas Branch, Islamic Azad University, Bandar Abbas, Iran. REZA DERAKHSHANDEH-HAGHIGHI is with the Department of Materials Science and Engineering, Shiraz Branch, Islamic Azad University, Shiraz, Iran. Contact e-mail: derakhshande@shirazu.ac.ir

Manuscript submitted 6 June, 2017.
Article published online January 30, 2018

inter-dendritic regions in fusion zone are enriched with Cr, Mo, and C. It leads to the precipitation of $M_{23}C_6$-type precipitates. Naffakh *et al.*[13] employed four different filler metals for welding Inconel 657 and 310 stainless steel. They reported that Inconel A filler material offers the optimum properties at room temperature. Successful defect-free joint of Inconel 625 to UNS 32205 duplex stainless steel was performed using electron beam welding by Ramkumar *et al.*[14] They reported a fine cellular dendritic structure at the fusion zone. The secondary phases and Mo-rich segregations at fusion zone impoverished the effect of electron beam welding on toughness and tensile strength. Wang *et al.*[15] investigated the microstructure in dissimilar welding of 316 stainless steel and Inconel 182. They found two alternately distributed typical fusion boundaries: a narrow random boundary and an epitaxial fusion which greatly affect microhardness. Microstructural features of dissimilar welds between 316LN austenitic stainless steel and alloy 800 were investigated by Sireesha *et al.*[16] These welds were produced using three types of filler materials such as austenitic stainless steels corresponding to 316, 16Cr–8Ni–2Mo, and the nickel-based Inconel 182. Dissimilar metal welds composed of low alloy steel, Inconel 82/182 weld, and stainless steel were prepared by GTAW and shielded metal arc welding (SMAW) techniques in the study of Jang *et al.*[17] Sayiram *et al.*[18] investigated the microstructure of dissimilar welds between Incoloy 800H and 321 stainless steel. The microscopic examination of the base metals, fusion zones, and interfaces revealed precipitates of Ti (C, N) in the austenitic matrix along the grain boundaries of the base metals.

So, most of the studies are based on 310 stainless steel which has higher amount of carbon than 316L stainless steel. On the other, hand 316L stainless steel has 2 to 3 wt pct. Mo which can affect microstructural and mechanical behavior of the weld. In spite of the industrial applications demanding the need for joining Inconel 625 and 316L stainless steel, no distinct work has been carried out on these dissimilar joints. It is worth investigating such dissimilar joints as they are widely used in transferring and injection of inhibitors in gas platforms. This article evaluates the influence of filler metals on structure–property relationships of GTA and shielded metal arc (SMA) weldments using different characterization techniques.

II. MATERIALS AND METHODS

The base materials used in this study were 6.02-mm-thick pipes of 316L stainless steel and Inconel 625 superalloy. The chemical composition of base materials and the filler metals was evaluated by emission spectroscopy analysis. The nominal chemical compositions of the base materials and the filler metals are given in Table I. In this study, SMAW and GTAW were performed to weld dissimilar metals. After removing all oxidation products at the contact area by brushing, a double groove was machined as shown in Figure 1. According to ASME B31.4,[19] the bevel angle for pipe welding is 37.5 ± 2.5 deg. So, 75 deg with $\pm$ 5 deg tolerance was chosen for groove angle (included angle) to fulfill this requirement. 75 deg is suitable for a trained welder to approach the root better. To avoid oxidation during DCEN-GTAW, shielding gas (Argon) with a purity of 99.9 pct and 8 L/min flow rate was utilized. A 2.4 mm 2 pct thoriated tungsten electrode and a 1.6 mm ERNiCrMo-3 and ERSS316L filler metal were used during GTAW. The torch angle was set as 70 deg.[20] Welding was conducted without weaving and string mode was applied. A 2.5 mm ENiCrMo-3 electrode was also used during DCEN-SMAW. The two examined consumables were Inconel 625 (ERNiCrMo-3 filler metal and ENiCrMo-3 Electrode) and 316L stainless steel (ERSS316L filler metal). By utilizing GTAW, no slag is present to contend with and generally the tie-ins at the toes of the root pass and starts/stops are very clean as well. That is providing that proper purge or other forms of internal protection are provided for the root and it is maintained long enough for the heat from other passes to be negated and not oxidize or otherwise contaminate the root surface. It is not practically more economical in industries to weld the root pass by SMAW. As far as comparing GTAW with SMAW was

Table I. Nominal Chemical Compositions of the Base Materials and the Filler Metals

	Base Metal		Filler Metal and Electrode		
Elements	Inconel 625	316L s.s	ERNiCrMo-3 Filler Metal	ERSS316L Filler Metal	ENiCrMo-3 Electrode
Cr	21.6	16.97	20.9	18.8	21.7
Ni	62.24	10.98	65.89	11.43	63.4
Fe	4.13	bal.	0.94	bal.	1.66
Mo	8.5	2.008	8.47	2.19	9.49
Nb	3.53	—	3.46	—	3.21
Mn	—	1.9	0.05	1.71	0.01
Ti	—	—	0.18	—	—
C	—	0.013	0.01	0.02	0.05
Cu	—	—	0.03	0.32	0.01
Si	—	0.27	0.05	0.44	0.46
S	—	—	0.001	0.01	0.007
P	—	0.022	0.019	0.017	0.002

the aim of the study, the whole passes including the root pass were welded by SMAW to be comparable with the ones welded just by GTAW.

Table II shows the welding voltage (E), current (I), welding speed (V), and total heat input which were recorded during welding. In the present study, after a weld pass was laid, the weld plate was allowed to cool down at a maximum interpass temperature of 150 °C for ERSS316L and 100 °C for ERNiCrMo-3 before the start of the next pass. During and after welding, the welds were visually inspected for their quality. It was ensured that the SMAW and GTAW weld beads possessed good geometrical consistency and were free from visible defects. According to macrographs shown in Figure 2, the only difference was the reinforcement length of the weld which is a bit longer in SMA-NiCrMo sample (Figure 2(a)) than GTA-NiCrMo sample (Figure 2(b)). Transverse sections of the welds after etching in marble solution (10 g $CuSO_4$ + 50 mL HCl + 50 mL H_2O) were characterized by optical and scanning electron microscopy. Chemical compositions of different points on SEM micrographs were determined by energy dispersive X-ray spectrometer (EDS). According to ASTM-E8 standard, transverse tensile test was performed at room temperature using GoTech machine. The samples were tested at a nominal strain rate of 0.2 mm/s at room temperature. Vickers microhardness (HV) measurements were made across different zones such as base metal, HAZ, and weld metal at a load of 1000 g with 15 s dwell time by using a Leitz microhardness tester. In order to obtain statistically reliable results, hardness and tensile tests were carried out using three specimens for each individual material testing. Absorbed impact energy measurements of the welds were determined by using Zwick Roell V-notch impact test machine at − 29 °C.

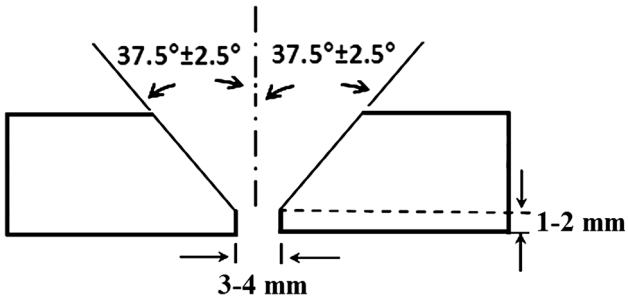

Fig. 1—Double groove joint design used in this study.

III. RESULTS AND DISCUSSION

A. *Base Metal Microstructure*

The microstructure of as-received Inconel 625 and 316L stainless steel is shown in Figures 3(a) and (b), respectively.

The microstructure of Inconel 625 comprises blocky carbides inside the grains or on the primary austenite grain boundaries. Fine stringer carbides are also present on the grain boundaries. Higher magnification of SEM micrograph (Figure 4) shows blocky and fine stringer carbides in the microstructure. EDS analysis of these carbides indicates large Mo-rich (Mo_6C) of type (M_6C) carbides (Figure 5(a)) along with fine Cr-rich ($Cr_{23}C_6$) of type ($M_{23}C_6$) carbides on the grain boundaries (Figure 5(b)). According to Figure 2(b), base metal in

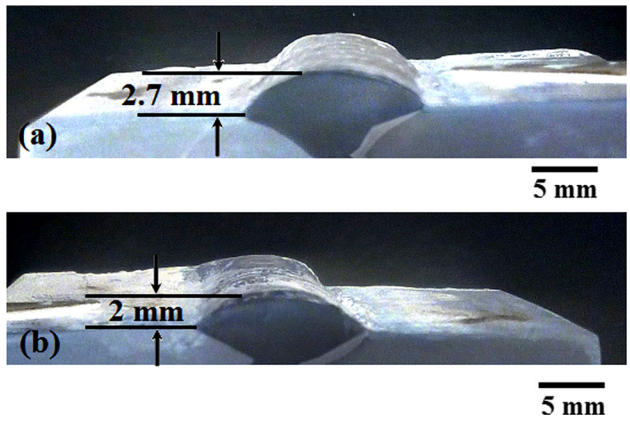

Fig. 2—Macrographs from the cross section of the welds (*a*) SMA-NiCrMo sample, (*b*) GTA-NiCrMo sample.

Table II. Welding Voltage (E), Current (I), Welding Speed (V), and Total Heat Input Recorded During Welding

Sample No.	Welding Method	Pass	Current(A)	Voltage (E)	Welding Speed, V (mm/s)	Heat Input (kJ/mm)	Total Heat Input (kJ/mm)
GTA-NiCrMo	GTAW	root	74	12	0.53	1.66	3.95
	GTAW	hot	91	29	2.83	0.91	
	GTAW	filling	92	30	2.12	1.38	
GTA-SS316L	GTAW	root	74	12	0.63	1.38	4.60
	GTAW	hot	107	14	1.05	1.35	
	GTAW	filling	111	14	0.81	1.87	
SMA-NiCrMo	SMAW	root	76	13	0.71	1.36	4.17
	SMAW	hot	109	14	0.98	1.54	
	SMAW	filling	111	13	1.09	1.27	

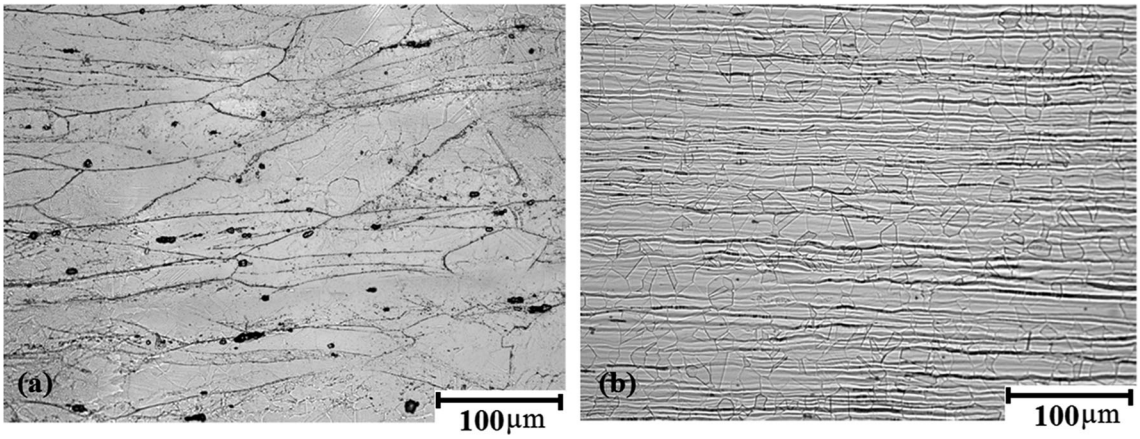

Fig. 3—Microstructure of (*a*) as-received Inconel 625 and (*b*) 316L stainless steel used in this study.

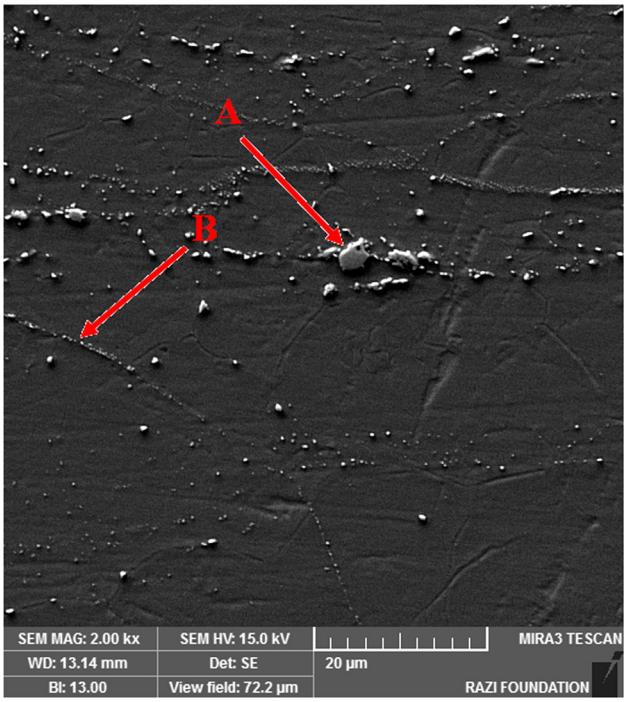

Fig. 4—SEM micrograph of Inconel 625 base metal with blocky and fine stringer carbides.

316L stainless steel comprises fine and equiaxed austenite grains with twin boundaries.

B. *Weld Metal Microstructure*

The fusion zone microstructure of sample GTA-NiCrMo welded by ERNiCrMo-3 filler metal is shown in Figures 6(a) and (b) with higher magnification. The microstructure is austenitic with inter-dendritic carbides. Mo and Nb show severe segregation during solidification of weld metal because their equilibrium distribution coefficient, k, is less than one.[21,22] Elements with $k < 1$, have a strong tendency for solute redistribution during solidification.[13,21] Constitutional super-cooling can occur due to reduction of temperature gradient at the solid/liquid interface when solute redistribution happens. This phenomenon changes the solidification mode from cellular to dendritic or equiaxed.[21,23]

Figure 7(b) shows SEM micrographs of sample GTA-NiCrMo weld metal in which changing the solidification mode from dendritic to equiaxed happens when moving from fusion line to the weld center line. The change in the morphology of dendrites is related to the G/R ratio (Temperature gradient, G, and solidification rate, R), that determines the solidification mode in the weld metal. Kou[1] has indicated that at a constant temperature gradient, the solidification rate is maximum at the weld center line and is minimum at the weld fusion line, so that $(G/R)_{CL} < (G/R)_{FL}$. By reducing (G/R) constitutional super-cooling increases and the solidification mode changes from dendritic to equiaxed. Higher magnification of dendritic and equiaxed zones are shown in Figures 7(a) and (c), respectively. At the terminal stage of solidification, Nb and Mo segregate to the liquid due to their low solubility in the austenite phase. So, the first solid is depleted from Mo or Nb at the dendritic cores and inter-dendritic regions get rich in Mo and Nb.

Figures 8(a) and (b) illustrate the EDS analysis of the inter-dendritic (arrow "A") and dendritic cores (arrow "B") of SEM micrograph shown in Figure 7(a), respectively. EDS analysis confirms that during solidification, Nb and Mo leave dendritic cores and are rejected to inter-dendritic regions. Sample GTA-SS316L was welded with ERSS316L filler metal. Since there are small amounts of elements with a high tendency for segregation in the composition of ERSS316L filler metal, the occurrence of constitutional super-cooling for changing the solidification mode from cellular to dendritic or equiaxed is less probable. So, according to Figures 9(a), the weld microstructure remains as columnar dendritic. δ-Ferrite appears in the microstructure in the inter-dendritic region of dendritic austenite as shown in Figure 9(b).

Figure 10(a) illustrates Laves phase in the weld metal of sample SMA-NiCrMo welded with ENiCrMo-3 electrode by using SMAW. EDS analysis of arrow "A" shown in Figure 10(b) confirms the presence of

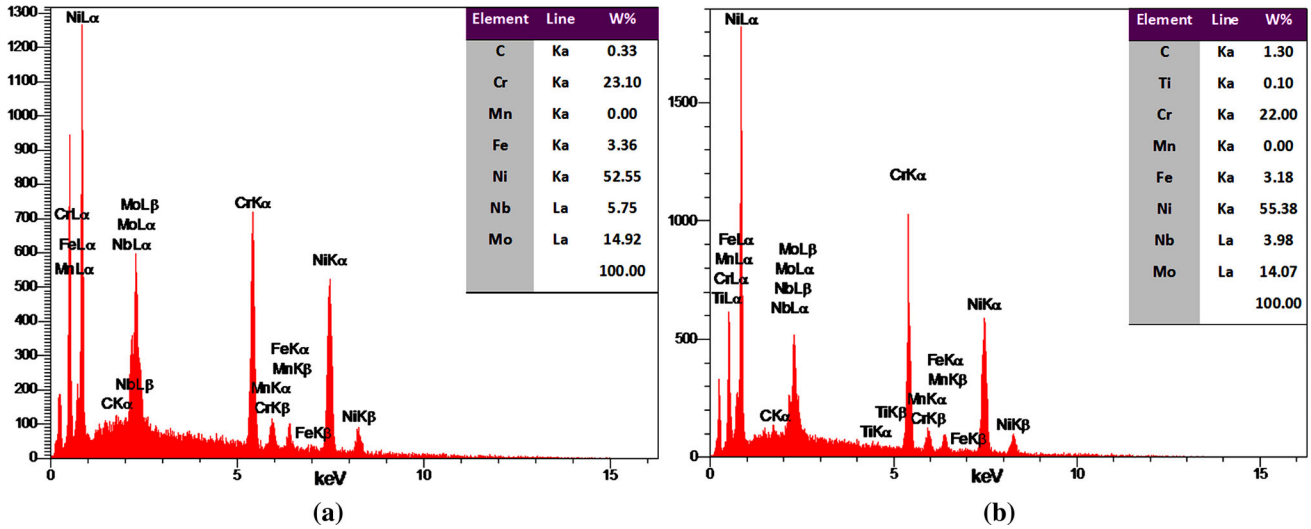

Fig. 5—EDS analysis of carbides in the microstructure (*a*) blocky carbides, (*b*) stringer carbides.

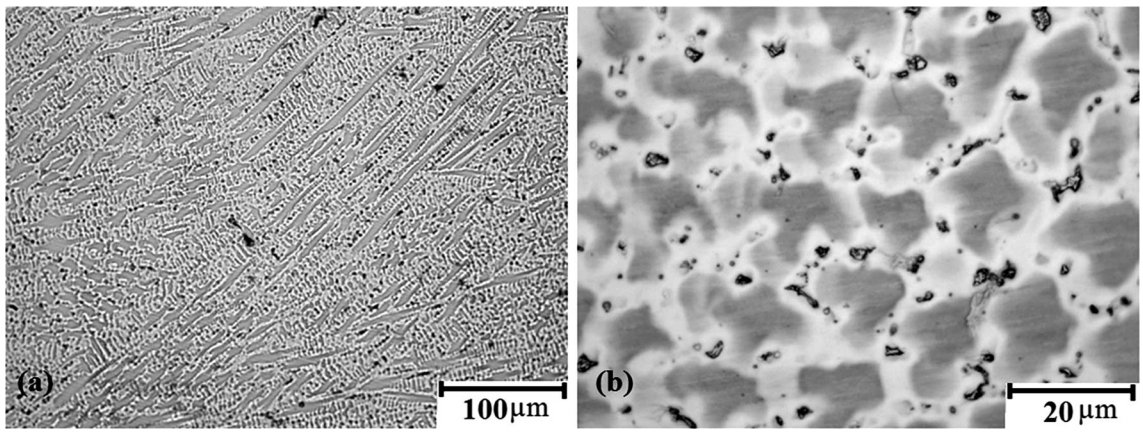

Fig. 6—(*a*) Austenite with inter-dendritic carbides in the fusion zone of sample GTA-NiCrMo welded by ERNiCrMo-3 filler metal, (*b*) weld metal microstructure of sample GTA-NiCrMo at higher magnification.

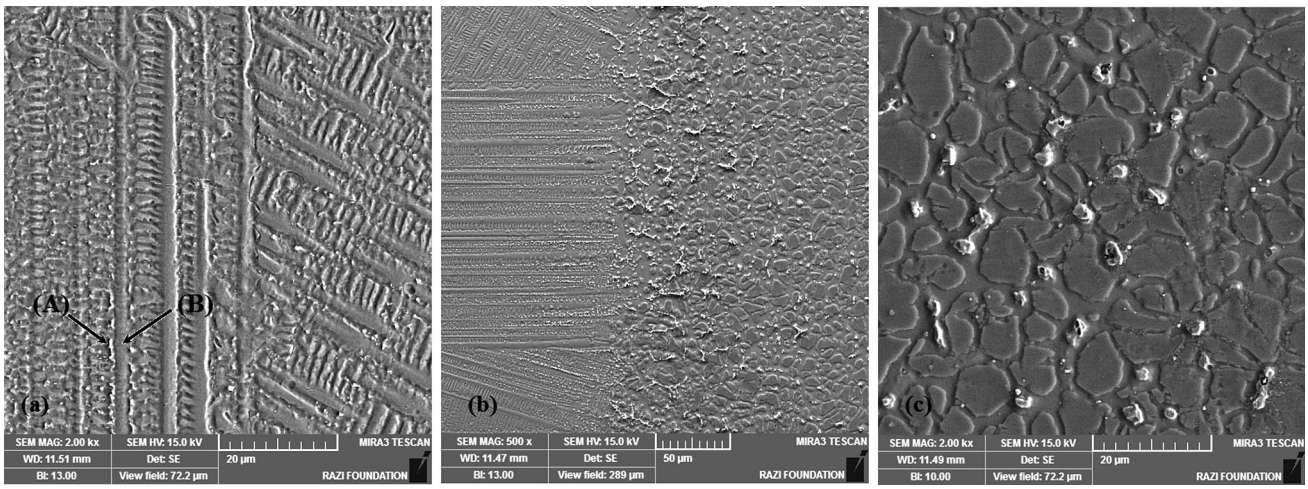

Fig. 7—(*a*) High magnification of dendritic microstructure of weld metal in sample GTA-NiCrMo, (*b*) changing the solidification mode from dendritic to equiaxed when moving from fusion line to the weld center line, (*c*) high magnification of equiaxed microstructure of weld metal in sample GTA-NiCrMo.

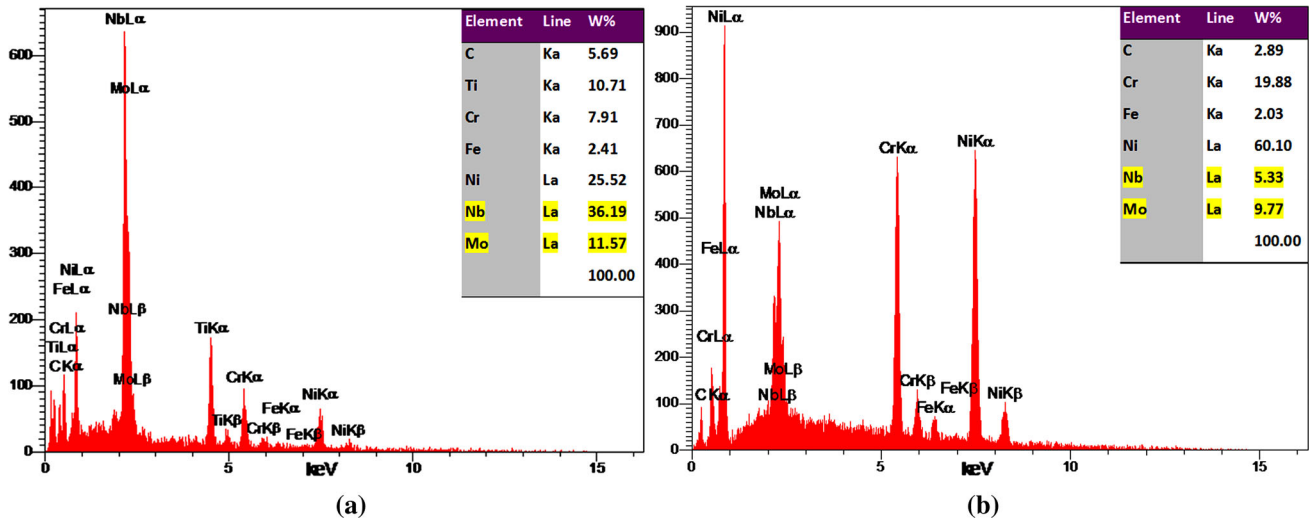

Fig. 8—EDS analysis of (*a*) inter-dendritic (arrow "A") and (*b*) dendritic cores (arrow "B") of SEM microstructure of weld metal in sample GTA-NiCrMo.

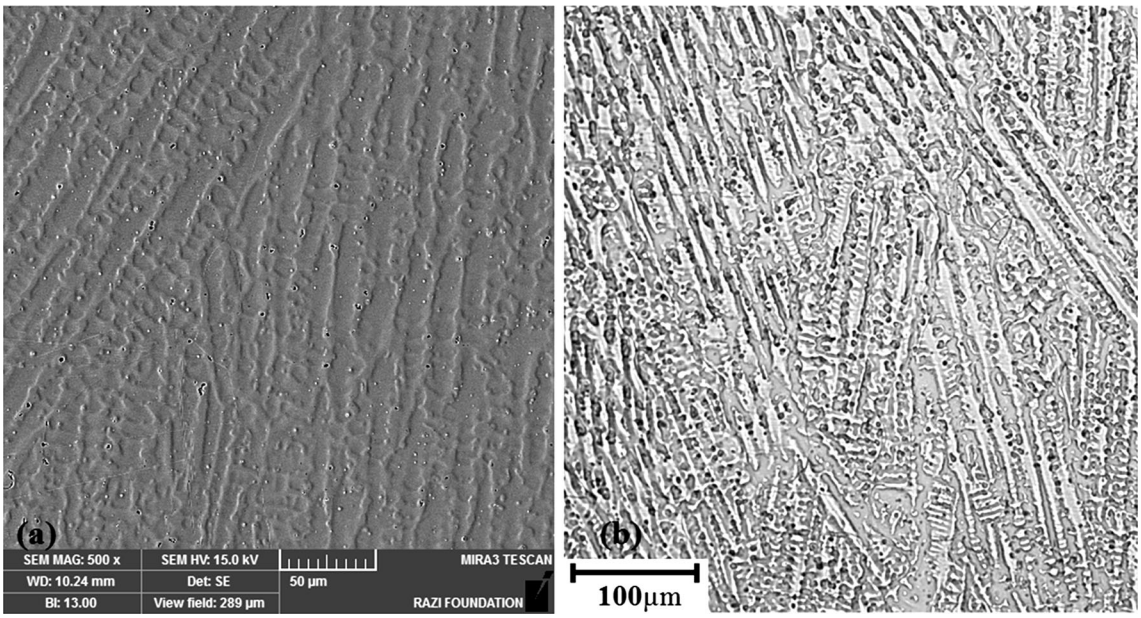

Fig. 9—Weld microstructure of sample GTA-SS316L welded with ERSS316L filler metal (*a*) SEM micrograph of columnar dendrites, (*b*) optical micrograph of δ-ferrite in the microstructure in the inter-dendritic region.

predominant elements such as Nb, Mo, Ni, Cr, and Fe for the formation of Laves phase in the weld metal. According to Reference 24, the segregation ratio (SR-ratio between alloy content in inter-dendritic liquid and dendritic solid) of Nb reduces with increased cooling rate, and segregation of Nb under lower cooling rates promotes more of Laves phase formation. Cooling rate increases by decreasing heat input. GTAW in comparison to SMAW produces lower heat input. Although weld metal composition for sample GTA-NiCrMo and sample SMA-NiCrMo is the same, the amount of heat input for sample SMA-NiCrMo is higher about 6 pct. This leads to the formation of Laves phase in sample SMA-NiCrMo. Using GTAW with lower heat input results in a higher cooling rate, and finer microstructure with smaller dendrite arm spacing is obtained. Figures 11(a) and (b) compares the weld metal microstructure of sample GTA-NiCrMo and sample SMA-NiCrMo, respectively.

Applying filler metals with richer alloying elements may have pronounced effect on mechanical properties of weld metals. However, some alloying elements such as Mo or Nb show severe segregation during solidification due to $k < 1$. It means that these elements are accumulated in liquid during solidification. So it is expected that relatively large amount of Mo or Nb will be enriched in the final liquid of fillers containing such elements. The relatively higher concentration of Nb in the inter-dendritic regions is very conducive to the formation of NbC compound. Segregation is a time-dependant phenomenon and is

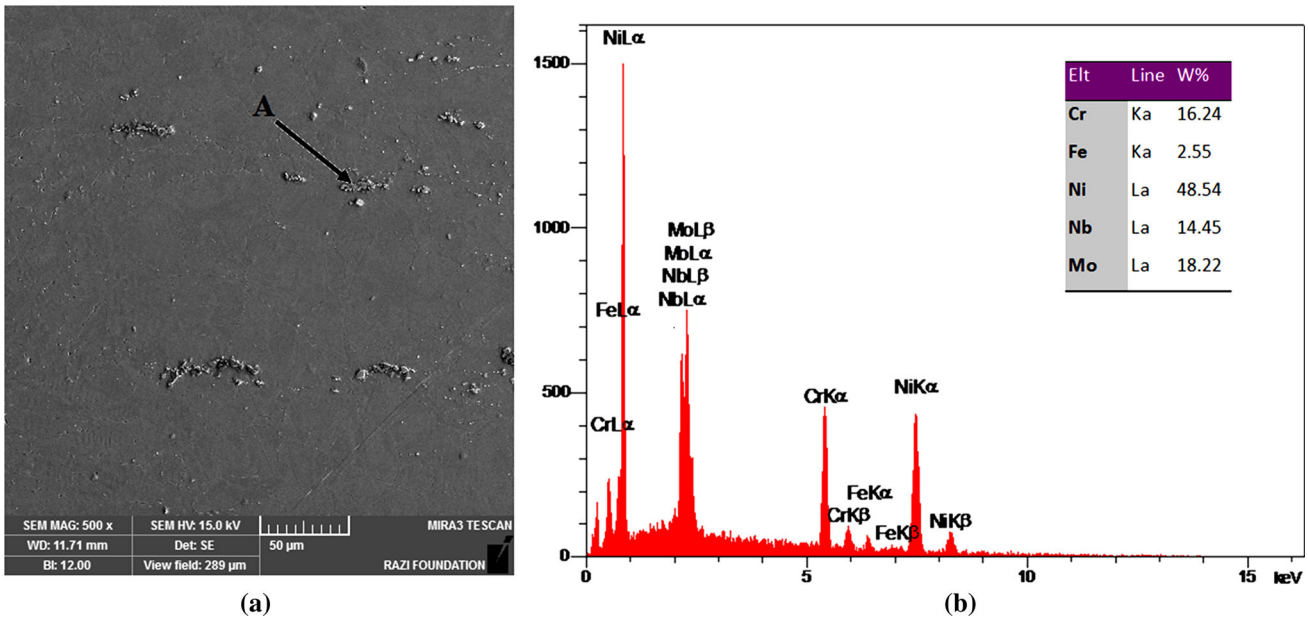

Fig. 10—(*a*) Presence of Laves phase in the weld metal of sample SMA-NiCrMo welded with ENiCrMo-3 electrode by using SMAW, (*b*) EDS analysis of arrow "A" in the microstructure.

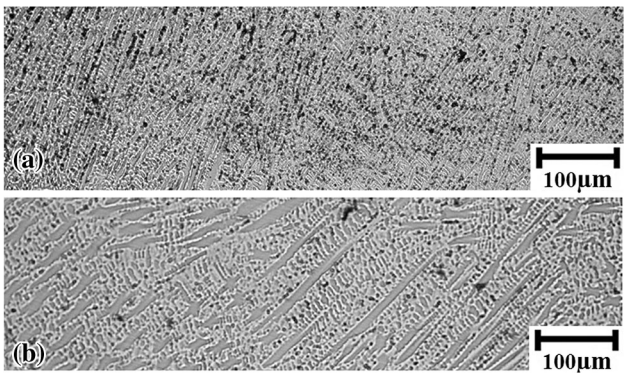

Fig. 11—Effect of heat input on weld metal microstructure (*a*) GTAW with small dendrite arm spacing in sample GTA-NiCrMo, (*b*) SMAW with large dendrite arm spacing in sample SMA-NiCrMo.

mainly influenced by cooling rate and heat input. When the weld metal cools slowly, there is sufficient time for redistribution of solute elements, thus the extent of micro-segregation is more. To minimize the effect of micro-segregation, using low heat input welding methods can be beneficial. Lower heat input results in higher cooling rate which helps in reducing the segregation of Nb and also reducing the formation of brittle Laves phase in inter-dendritic regions. According to the mechanism reported in literature,[25] the solidification temperature of NbC (1325 °C) is higher than that of the laves (1266 °C). The NbC firstly nucleates and grows in the form of (γ + NbC). As the solidification progresses, Nb is aggregated in front of the liquid/solid interface. When the local Nb/Cr ratio becomes larger, (γ + laves) appears and results in γ/laves eutectic microstructure. According to Reference 26, Fe increases the segregation potential of Nb by reducing equilibrium distribution coefficient, k. Thus, Fe addition reduces the solubility of Nb in the γ matrix. 316L stainless steel and Inconel 625 both have enough Fe amount to reduce Nb solubility and to aggravate inter-dendritic micro-segregation of Nb. This phenomenon also influences on Mo partition coefficient based on Reference 13 studies. Thus, as the amount of Fe in the weld increases (*i.e.*, as the dilution level is increased) Mo solubility decreases. According to the mechanism stated by Banovic *et al.*,[22] when cooling rate decreases by increasing heat input the dendrite or cell size increases and the distance over which the solute will travel to compensate the composition gradient through the dendrite core increases. Mo has low diffusion rate in the austenite phase which causes the Mo to micro-segregate to the liquid phase leaving the first solid depleted in Mo. The low diffusion rate of Mo in austenite does not allow Mo to diffuse back to the solid to compensate for the composition gradient. As the solidification proceeds, the dendrites grow in size leaving the surrounding liquid enriched in Mo.

C. *Microstructural Characterization of Interfaces*

The interface between Inconel 625 base metal and ERNiCrMo-3 weld metal is shown in Figure 12(a). No considerable unmixed zones can be observed in this figure. It can be attributed to more dilution and the similarity of filler and base metal from the viewpoint of the melting temperature and chemical composition. However, the interface between 316L stainless steel base metal and ERNiCrMo-3 weld metal shown in Figure 12(b) is a large unmixed zone. The existence of unmixed zones has caused severe concern in the welding industry[27–29] due to detrimental influence of this zone on corrosion resistance of the weld. It is often important for the cases that alloys with high levels of molybdenum,

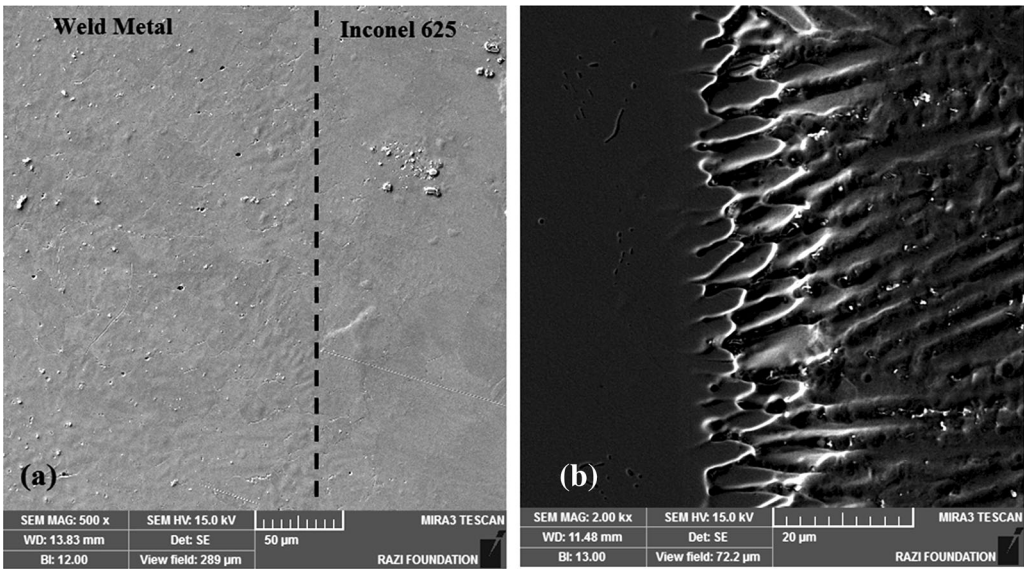

Fig. 12—(*a*) Interface between Inconel 625 base metal and ERNiCrMo-3 weld metal with no considerable unmixed zones, (*b*) Interface between 316L stainless steel base metal and ERNiCrMo-3 weld metal with large unmixed zone.

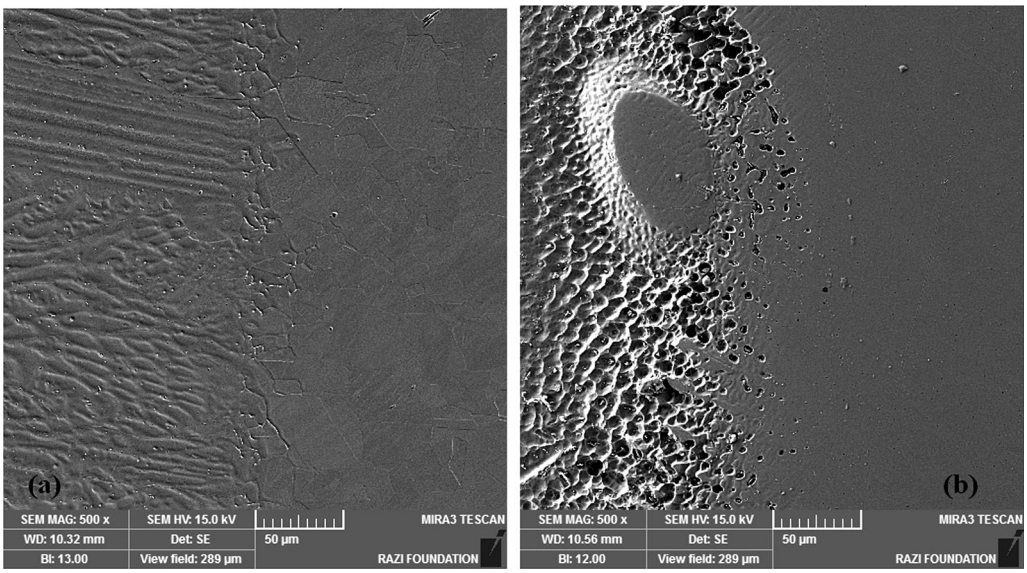

Fig. 13—(*a*) Interface between 316L stainless steel base metal and ERSS316L weld metal with no detectable unmixed zone, (*b*) extensive unmixed zone between Inconel 625 base metal and ERSS316L weld metal.

chromium, and nickel need to have high corrosion resistance in aggressive environments. When the melting range of filler materials is similar to or higher than that of the base metal, only a small fraction of the base metal can be melted and no filler metal dilution occurs in the re-solidification stage and no unmixed zone is formed.[30,31]

The interface between 316L stainless steel base metal and ERSS316L weld metal is shown in Figure 13(a) with no detectable unmixed zone; whereas an extensive unmixed zone is formed between Inconel 625 base metal and ERSS316L weld metal as shown in Figure 13(b). This is because of this fact that the convection currents are not able to promote adequate fluid flow and mixing, so lack of dilution occurs. An epitaxial growth is also visible at the interface of 316L stainless steel base metal and ERSS316L weld metal as shown in Figure 14 where the chemical composition of filler metal and base metal is the same. Away from the fusion line, the grain structure is dominated by competitive growth.[24] During weld metal solidification, grains tend to grow in the direction perpendicular to pool boundary because this is the direction of maximum heat extraction. In this way, grains will grow more easily and crowd out less favorably oriented grains as shown in Figure 14.

Figure 15 shows the unmixed zone between 316L stainless steel base metal and ERNiCrMo-3 weld metal performed by GTAW and SMAW. According to this figure, the unmixed zone in sample GTA-NiCrMo (Figure 15(a)) is narrower than sample SMA-NiCrMo (Figure 15(b)). Higher heat input with lower cooling rate in SMAW method (sample SMA-NiCrMo) provides longer time for diffusion of elements such as Mo, Nb, and Cr to both sides and widening of unmixed zone occurs. As shown, higher amounts of bright precipitates are present in the unmixed zone of sample GTA-NiCrMo due to lack of enough time for diffusion to different sides.

Based on Figures 16(a) and (b), grain coarsening is clearly shown in HAZ of sample GTA-NiCrMo and sample SMA-NiCrMo at Inconel side, respectively. Higher heat input by using SMAW, shown in Figure 16(b), leads to an outstanding HAZ grain coarsening in comparison to utilizing GTAW, shown in Figure 16(a). HAZ experiences higher temperature than base metal, so most of the precipitates in this region are eliminated and larger ones are formed. Figure 17(a) displays the carbide elimination in Inconel 625 HAZ and Figure 17(b) shows an optical micrograph of this region with coarse carbides along with fine carbides on the grain boundaries. Controlling interpass temperature is necessary to prevent from precipitation of undesirable carbide or intermetallic phases in the HAZ. Carbides generally precipitate in the grains or along grain boundaries. These carbides impair creep life, ductility, and corrosion resistance.[32] Low-melting-point films can form along the solidification grain boundaries due to segregation of alloying elements. The strain that develops during weld solidification separates the grain boundaries which leads to cracks.[33,34] When stainless steel is exposed to higher temperatures and longer times, the HAZ is sensitized. In sensitization chromium precipitates out at the grain boundaries in the form of carbides leaving the surrounding area depleted of corrosion-resisting elements.[32] So, according to above reasons, interpass temperature was kept as low as possible. The prediction of inter-dendritic micro-segregation is possible for fillers containing Mo or Nb. When dealing with alloys containing high amount of Fe, the reduction in Mo and Nb solubility in the γ matrix is accentuated. So, segregation of Nb and Mo under lower cooling rates promotes more of Laves phase formation. However, sometimes utilizing filler metals with lower amount of elements with high segregation tendency is not possible. This is because of this fact that various alloying elements are purposely added to filler metals for solid solution strengthening like Mo or for precipitate formation like Nb. These alloying elements can improve mechanical properties of the weld and can avoid crack nucleation in the weld metal. Thus, selecting

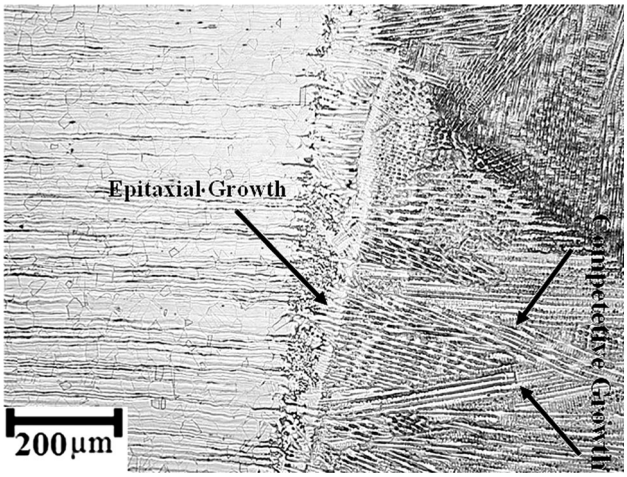

Fig. 14—Epitaxial growth at the interface of 316L stainless steel base metal and ERSS316L weld metal.

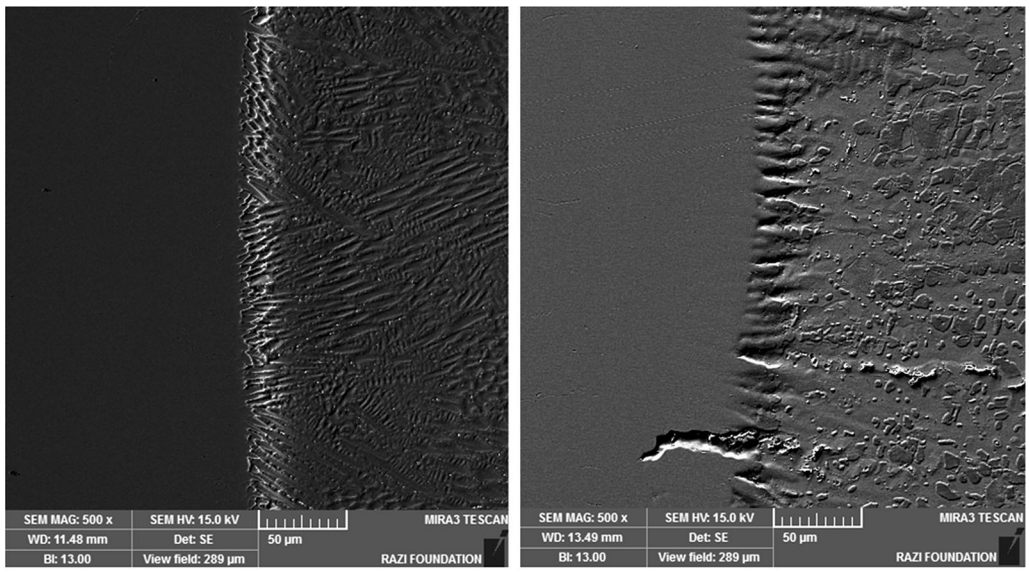

(a) (b)

Fig. 15—Unmixed zone between 316L stainless steel base metal and ERNiCrMo-3 weld metal performed by (*a*) GTAW and (*b*) SMAW.

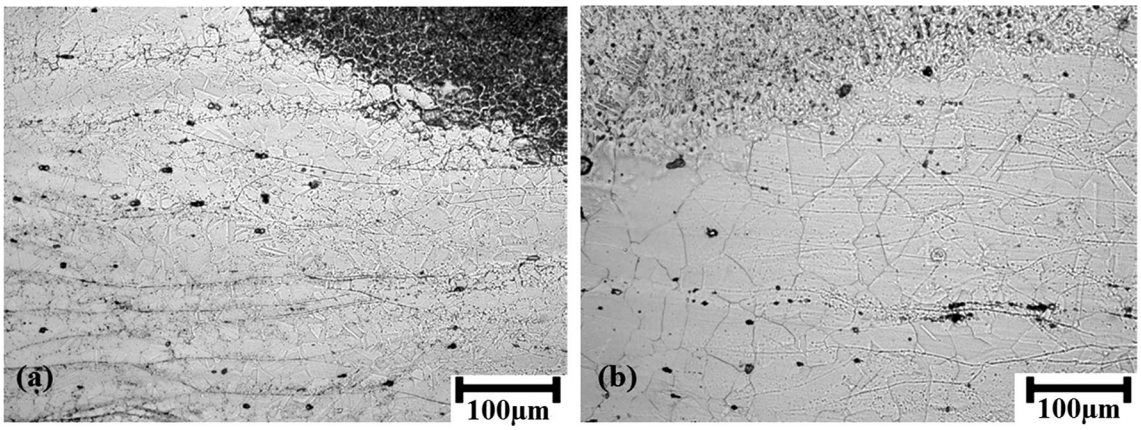

Fig. 16—Grain coarsening in Inconel 625 HAZ of (*a*) sample GTA-NiCrMo welded by GTAW and (*b*) sample SMA-NiCrMo welded by SMAW.

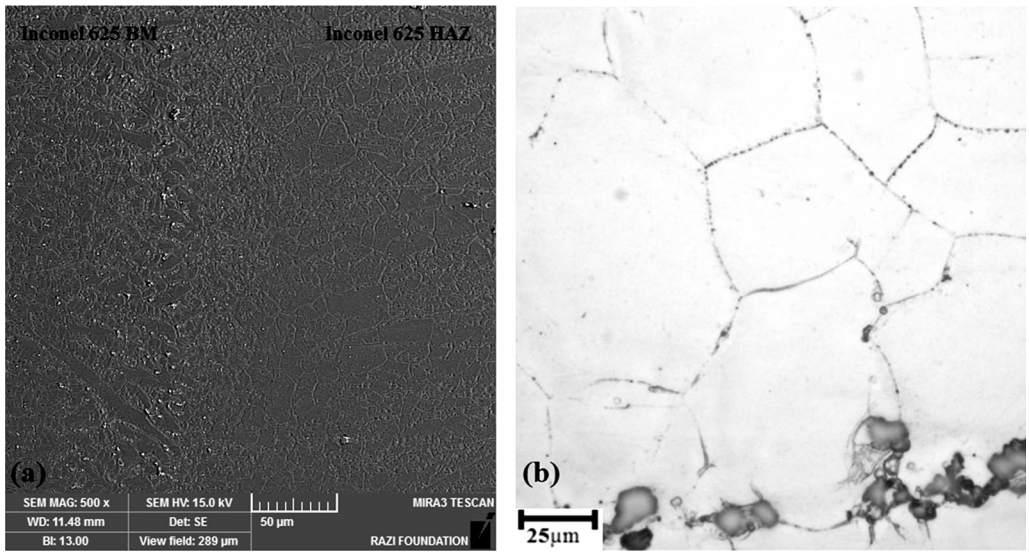

Fig. 17—(*a*) SEM micrograph of carbide elimination in Inconel 625 HAZ, (*b*) optical micrograph of this region with coarse carbides along with fine carbides on the grain boundaries.

ERNiCrMo-3 filler metal is more advantageous than ER316L filler metal. Fe can reduce Mo and Nb solubility in the γ matrix. Fe content of the weld is controlled by dilution and dilution is controlled by welding parameters. So, different welding parameters such as heat input have direct influence on the micro-segregation of Mo or Nb. Applying lower heat input methods such as GTAW in comparison to SMAW will be helpful in increasing cooling rate and reducing the probability of brittle Laves phase formation. Furthermore, higher cooling rate results in finer dendritic microstructure and less grain growth.

D. *Assessment of Mechanical Properties*

Tensile test results of welded joints are shown in Table III along with the properties of both base metals. According to literature,[35,36] the minimum (UTS and YS) for Inconel 625 and 316L stainless steel base metals are (710 and 350 MPa) and (559 and 304 MPa), respectively. These tensile properties are in accordance with the data given in Table III. Fracture after tensile test in sample GTA-NiCrMo and sample SMA-NiCrMo occurred in 316L heat-affected zone (HAZ) where extensive grain growth takes place. However, failure occurs in weld metal (WM) for sample GTA-SS316L where weld metal strength is lower than the other base metals. The results show that sample GTA-NiCrMo exhibits the highest UTS and elongation. The minimum UTS and elongation is obtained with ERSS316L filler metal in sample GTA-SS316L. Sample SMA-NiCrMo shows lower UTS and elongation than sample GTA-NiCrMo. This is because of larger grains in HAZ and coarser microstructure obtained by SMAW as was mentioned previously (Figures 11 and 16).

Variations of hardness across the welds are shown in Figure 18. ERNiCrMo-3 weld metals exhibited higher

Table III. Tensile Test and Impact Test Results of Different Samples Used in this Study

Sample No.	Material	Yield Strength (MPa)	Ultimate Tensile Strength (MPa)	Total Elongation (pct)	Impact Energy (J)	Failure Location After Tensile Test
—	Inconel 625 base metal	390 ± 10	844 ± 9	40 ± 6	91 ± 4	—
—	316L base metal	310 ± 2	578 ± 2	45 ± 4	95 ± 2	—
GTA-NiCrMo	GTAW (ERNiCrMo-3 filler metal)	249 ± 14	645 ± 7	34 ± 4	60 ± 2	316L HAZ
GTA-SS316L	GTAW (ERSS316L filler metal)	231 ± 18	552 ± 14	21 ± 3	41 ± 4	WM
SMA-NiCrMo	SMAW (ENiCrMo-3 electrode)	249 ± 8	628 ± 6	31 ± 3	30 ± 5	316L HAZ

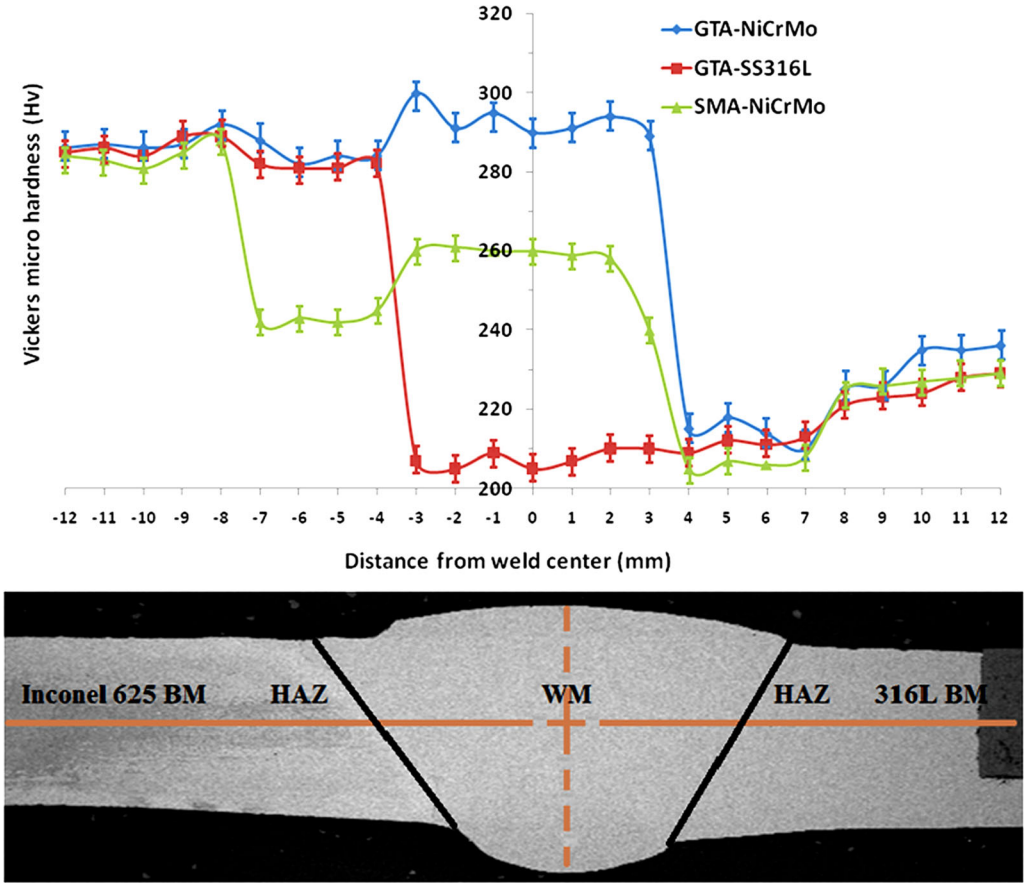

Fig. 18—Variation of hardness results in transverse cross section of the welds.

hardness values than 316L base metal due to their intrinsic higher hardness, whereas Inconel 625 base metal shows higher hardness value than the whole weld metals. Sample GTA-NiCrMo (GTAW, ERNiCrMo-3 filler metal) exhibits the highest hardness value among the weld metals studied and sample GTA-SS316L (GTAW, ERSS316L filler metal) shows the lowest hardness value. This large difference is attributed to the chemical composition of the filler metals. At the terminal stage of solidification of ERNiCrMo-3 weld metal, Nb and Mo segregate to the liquid due to their low solubility in the austenite phase and carbides with high hardness are produced. In fact rejection of Nb into inter-dendritic regions during solidification along with diffusion of carbon by an interstitial mechanism can produce NbC. However, microstructure of solidified of ERSS316L filler metal is composed of columnar austenite with a little δ-ferrite which definitely has lower microhardness. It can also be observed that the microhardness value decreases from Inconel 625 base metal to HAZ for all the samples. It is the evidence for carbide coarsening or carbide dissolution in HAZ (Figure 17). Sample SMA-NiCrMo experiences higher heat input and grain growth occurs. So, HAZ microhardness for sample SMA-NiCrMo is lower than sample GTA-NiCrMo.

The Charpy test results for as-welded specimens are listed in Table III. In addition, toughness values of base metals are included for comparison. Sample GTA-NiCrMo exhibited the highest impact energy. In contrast, sample SMA-NiCrMo shows the least toughness. This remarkable difference in absorbed impact energy is mainly because of the presence of Laves phase in SMA-NiCrMo weld metal as was previously discussed. The detrimental effect of the hard precipitates like Laves phase on the impact toughness was also reported in the weld metals of other nickel-based alloys.[37–39] Rapid solidification of ERSS316L filler metal in sample GTA-SS316L leads to the formation of δ-ferrite in the microstructure. Due to the presence of ferrite promoting elements such as chromium, this ferrite segregates. Ferrite segregation may have deleterious effect on toughness of austenitic stainless steel.[40] So, absorbed impact energy of the ERSS316L weld metal is less than 316L base metal.

IV. CONCLUSION

Dissimilar joints between Inconel 625 superalloy and 316L stainless steel are widely used in transferring and injection of inhibitors in gas platforms. This article evaluates the influence of filler metals on structure–property relationships of GTA and SMA weldments using different characterization techniques. The conclusions are as follows

1. During ERNiCrMo-3 weld metal solidification, Nb and Mo leave dendritic cores and are rejected to inter-dendritic regions in both welding methods.
2. The segregation ratio of Nb increases with decreasing cooling rate and higher Nb segregation promotes more of Laves phase formation that decreases absorbed impact energy.
3. The unmixed zone between 316L stainless steel base metal and ERNiCrMo-3 weld metal performed by GTAW is narrower than the one performed by SMAW.
4. Sample GTA-NiCrMo welded with ERNiCrMo-3 filler metal by GTAW exhibits the highest UTS, elongation, and absorbed impact energy. The minimum UTS, elongation, and absorbed impact energy are obtained with ERSS316L filler metal in sample GTA-SS316L. Moreover, sample SMA-NiCrMo shows lower UTS, elongation, and absorbed impact energy than sample GTA-NiCrMo because of larger grains in HAZ and coarser microstructure obtained by SMAW.
5. It can be concluded that using ERNiCrMo-3 filler metal along with GTA welding results in the best mechanical and metallurgical properties for joining Inconel 625 superalloy and 316L stainless steel.

ACKNOWLEDGMENTS

The authors thank the support from Islamic Azad University for providing the funding for this research.

REFERENCES

1. S. Kou: *Welding Metallurgy*, 2nd ed., Wiley-Inter Science, New York, 2003.
2. R. Avery: *Pay Attention to Dissimilar-Metal Welds: Guidelines for Welding Dissimilar Metals*, Avery Consulting Associates Inc, Toronto, Ont, 2003, pp. 1–6.
3. H.T. Lee, S.L. Jeng, C.H. Yen, and T.Y. Kuo: *J. Nucl. Mater.*, 2004, vol. 335, pp. 59–69.
4. T. Shoji, G.F. Li, J.H. Kwon, S. Matsushima, and Z.P. Lu: Proceedings of the 11th International Conference on Environmental Degradation of Materials Nuclear Power Systems—Water Reactors, ANS 2003, pp. 834–43.
5. P.M. Scott and P. Combrade: Proceedings of the 11th International Conference on Environmental Degradation Materials Nuclear Power Systems- Water Reactors, ANS 2003, pp. 29–38.
6. C.T. Sims, N.S. Stollof, and W.C. Hagel: Superalloys, 2nd ed., Wiley-Inter Science, New York, 1987.
7. V. Shankar, K.B.S. Rao, and S.L. Mannan: *J. Nucl. Mater.*, 2001, vol. 288, pp. 222–32.
8. P. Mithilesh, D. Varun, A. Reddy, G. Reddy, K. Devendranath Ramkumar, N. Arivazhagan, and S. Narayanan: *Procedia Eng.*, 2014, vol. 75, pp. 66–70.
9. H. Shah Hosseini, M. Shamanian, and A. Kermanpur: *Int. J. Press. Vessels Pip.*, 2016, vol. 144, pp. 18–24.
10. H. Shah Hosseini, M. Shamanian, and A. Kermanpur: *Mater. Charact.*, 2011, vol. 62, pp. 425–31.
11. A. Mortezaie and M. Shamanian: *Int. J. Press. Vessels Pip.*, 2014, vol. 116, pp. 37–46.
12. A.H.V. Pavan, K.S.N. Vikrant, R. Ravibharath, and K. Singh: *Mater. Sci. Eng. A*, 2015, vol. 642, pp. 32–41.
13. H. Naffakh, M. Shamanian, and F. Ashrafizadeh: *J. Mater. Process. Technol.*, 2009, vol. 209, pp. 3628–39.
14. K. Devendranath Ramkumar, R. Sridhar, S. Periwal, S. Oza, V. Saxena, P. Hidad, and N. Arivazhagan: *Mater. Des.*, 2015, vol. 68, pp. 158–66.
15. W. Wang, Y. Lu, X. Ding, and T. Shoji: *Mater. Charact.*, 2015, vol. 107, pp. 255–61.
16. M. Sireesha, V. Shankar, K. Albert Shaju, and S. Sundaresan: *Mater. Sci. Eng. A*, 2000, vol. 292, pp. 74–82.
17. C. Jang, J. Lee, J.-S. Kim, and T.-E. Jin: *Int. J. Press. Vessels Pip.*, 2008, vol. 85, pp. 635–46.
18. G. Sayiram and N. Arivazhagan: *Mater. Charact.*, 2015, vol. 102, pp. 180–88.
19. ASME code for pressure piping, ASME.B31.4, The American Society of Mechanical Engineers, New York, 2012, p. 50.
20. M. Abid, S. Parvez, and D.H. Nash: *Int. J. Press. Vessels Pip.*, 2013, vols. 108–109, pp. 51–60.
21. J.N. Dupont, J.C. Lippold, and S.D. Kiser: *Welding Metallurgy and Weldability of Nickel Base Alloys*, Wiley, New Jersey, 2009.
22. S.W. Banovic, J.N. DuPont, and A.R. Marder: *Sci. Technol. Weld. Join.*, 2002, vol. 6, pp. 274–83.
23. W.C. Winegard: *An Introduction to the Solidification of Metals*, Institute of Metals, London, 1964.
24. S.G.K. Manikandan, D. Sivakumar, K.P. Rao, and M. Kamaraj: *J. Mater. Process. Technol.*, 2014, vol. 214, pp. 358–64.
25. C.C. Silva, H.C. Miranda, M.F. Motta, J.P. Farias, C.R.M. Afonso, and A.J. Ramirez: *J. Mater. Res. Technol.*, 2013, vol. 2, pp. 228–37.
26. J.N. DuPont, C.V. Robino, and A.R. Marder: *Metall. Mater. Trans. A*, 1998, vol. 29A, pp. 2797–2806.
27. D.K. Aidun and J.P. Dean: *Weld. J.*, 1999, vol. 78, pp. 349–54.
28. A. Gutierrez and J.C. Lippold: *Weld. J.*, 1998, vol. 77, pp. 123–32.
29. A. Gutierrez, J.C. Lippold, and W.G. Lin: Welds*Mater. Sci. Forum*, 1996, vol. 217, pp. 1691–96.
30. M. Sireesha, S.K. Albert, V. Shankar, and S. Sundaresan: *J. Nucl. Mater.*, 2000, vol. 279, pp. 65–76.
31. R. Dehmolaei, M. Shamanian, and A. Kermanpur: *Mater. Charact.*, 2008, vol. 59, pp. 1447–54.
32. W. Mankins and S. Lamb: Nickel and nickel alloys. in Properties and Selection: Nonferrous Alloys and Special Purpose Materials, Metals Handbook, 10th ed, ASM International, London, 1990, pp. 428–45.
33. M.D. Rowe, P. Crook, and G.L. Hoback: *Weld. J.*, 2003, vol. 82, pp. 313–20.
34. S.C. Ernst: *Weld. J.*, 1994, vol. 73, pp. 80–89.

35. J.R. Davis: *ASM Specialty Handbook: Heat Resistance Materials*, 2nd ed., ASM International, Materials Park, 1999, p. 241.
36. R.M. Molak, K. Paradowski, T. Brynk, L. Ciupinski, Z. Pakiela, and K.J. Kurzydlowski: *Int. J. Press. Vessels Pip.*, 2009, vol. 86, pp. 43–47.
37. H.T. Lee, S.L. Jeng, and T.Y. Kuo: *Metall. Mater. Trans. A*, 2003, vol. 34, pp. 1097–1105.
38. T.Y. Kuo, H.T. Lee, and C.C. Tu: *Sci. Technol. Weld. Join.*, 2003, vol. 8, pp. 39–48.
39. H. Wang and G. He: *Mater. Sci. Eng. A*, 2016, vol. 672, pp. 15–22.
40. J.C. Lippold and D.J. Koteki: *Welding Metallurgy and Weldability of Stainless Steels*, Wiley, New Jersey, 2005.